

## Divergent trends in grassland degradation and desertification under land use and climate change in Central Asia from 2000 to 2020

Yanbo Zhao<sup>a</sup>, Jie Wang<sup>a,\*</sup>, Geli Zhang<sup>b</sup>, Luo Liu<sup>c</sup>, Jilin Yang<sup>a</sup>, Xiaocui Wu<sup>d</sup>, Chandrashekhar Biradar<sup>e</sup>, Jinwei Dong<sup>f</sup>, Xiangming Xiao<sup>g</sup>

<sup>a</sup> College of Grassland Science and Technology, China Agricultural University, Beijing 100193, China

<sup>b</sup> College of Land Science and Technology, China Agricultural University, Beijing 100193, China

<sup>c</sup> Guangdong Province Key Laboratory for Land Use and Consolidation, South China Agricultural University, Guangzhou 510642, China

<sup>d</sup> Department of Natural Resources and Environmental Sciences, University of Illinois at Urbana-Champaign, Urbana, IL 61801, USA

<sup>e</sup> Center for International Forestry Research (CIFOR) and World Agroforestry Center (ICRAF), Asia Continental Program, New Delhi, India

<sup>f</sup> Key Laboratory of Land Surface Pattern and Simulation, Institute of Geographic Sciences and Natural Resources Research, Chinese Academy of Sciences, Beijing 100101, China

<sup>g</sup> Department of Microbiology and Plant Biology, Center for Earth Observation and Modeling, University of Oklahoma, Norman, OK 73019, USA

### ARTICLE INFO

#### Keywords:

Climate change  
Drylands  
Desertification  
Grassland degradation  
Attribution analyses

### ABSTRACT

Grassland degradation (within-state change) and desertification (state conversion from grasslands to deserts) are different states in the complex dynamic process of grassland deterioration. However, the dynamics and associated drivers of the two states have been rarely examined separately, which is critical for early warning and conservation policy making. Here, the grassland degradation and desertification in Central Asia (CA) were studied due to their evident vulnerability to climate extremes and human activities. We performed a two-step approach to identify the critical state zones first (i.e., grasslands, deserts, and the desertification zones) and then assess the vegetation dynamics within each zone. Finally, we quantified the roles of CO<sub>2</sub> fertilization effect, climate change, climate variability, land use (LU), and anthropogenic climate change (ACC) on the vegetation dynamics in different state zones. The results showed that the areas of grasslands and sparse vegetation regions (including deserts and desertification zones) were stable from 2000 to 2020, but the trends of vegetation greenness were divergent with a reduction in grasslands and an increase in sparse vegetation regions. Furthermore, climate change and climate variability were the main driving force affecting grassland degradation in CA. Yet the vegetation greening in the desertification and desert zones was mainly driven by the rising CO<sub>2</sub> and LU. Moreover, ACC degraded 20.63% of grasslands and sparsely vegetated lands in CA on the baseline of 2000. The results highlighted the risks of grassland degradation in CA. This study proposed a methodology to examine grassland degradation and desertification in detail and quantify the associated driving factors (especially ACC) at the pixel scale, which provided some insights on developing region-precise strategies for grassland conservation in CA and other drylands.

### 1. Introduction

Drylands cover around 41% of the land surface and support over 38% of the human beings (Berduo et al., 2017; Reynolds et al., 2007), contributing to the largest variability in the global carbon sink and providing wide ecosystem services (Li et al., 2021; Lian et al., 2021; Poulter et al., 2014). Human activities pose a serious threat to vegetation habitats in global drylands, such as the loss of green space caused by urbanization (Cetin and Sevik, 2016; Ren et al., 2022; Yucedag et al.,

2018). In addition, climate change also largely affects the dryland vegetation growth. For example, drought led to the water shortage and soil productivity decline (Varol et al., 2023). Thus, dryland ecosystems are increasingly endangered by land degradation and desertification, which furthermore threatens the environment and socio-economic activities (Koutroulis, 2019; Reynolds et al., 2007). Grasslands, as the main ecosystem of drylands, are under severe threat from ongoing degradation undermining their capacity to support biodiversity, ecosystem services and human well-being (Bardgett et al., 2021).

\* Corresponding author at: College of Grassland Science and Technology, China Agricultural University, Yuanmingyuan West Road 2, Beijing 100193, China.  
E-mail address: [jiewang178@cau.edu.cn](mailto:jiewang178@cau.edu.cn) (J. Wang).

<https://doi.org/10.1016/j.ecolind.2023.110737>

Received 14 April 2023; Received in revised form 14 July 2023; Accepted 25 July 2023

Available online 27 July 2023

1470-160X/© 2023 The Authors. Published by Elsevier Ltd. This is an open access article under the CC BY-NC-ND license (<http://creativecommons.org/licenses/by-nc-nd/4.0/>).

Central Asia (CA) is one of the largest dryland regions, dominated by moisture-limited grassland, semi-desert, and desert ecosystems (Zhang et al., 2018). In the last 30 years, CA has been experiencing a higher warming rate (0.4 °C per decade) than the average (0.3 °C per decade) of the Northern Hemisphere (Hu et al., 2014; Ma et al., 2021). In addition, human activities in this region have changed dramatically since 1990, including the conversion of land reclamation and cropland abandonment, exploitation of gas and oil, and the rehabilitation of grazing activities (Karnieli et al., 2008; Zhou et al., 2019). These evident anthropogenic activities greatly affected the grassland conditions (Karnieli et al., 2008; Wright et al., 2012). Faced with significant increases in temperature, precipitation extremes, and dramatic land use changes (de Beurs et al., 2015; Hu et al., 2014; Schiemann et al., 2008), the grasslands are under increasing pressure of degradation and desertification in CA. In contrast, recent studies suggested that the global drylands experienced widespread greening driven by CO<sub>2</sub> fertilization or land use practices (Ahlström et al., 2015; Andela et al., 2013; Fensholt et al., 2012; He et al., 2019; Piao et al., 2020; Wang et al., 2018c). So far little is known about how the grassland states in CA response to the seemingly conflicting contexts. It is necessary to clarify the dynamics and the underlying driving mechanisms of grassland degradation and desertification in CA to improve our understanding and support the Sustainable Development Goal of zero net land degradation (SDG 15.3) in drylands (Jiang et al., 2022).

According to the desertification theory in the framework of bi-stable ecosystem dynamics, there are critical thresholds (or tipping points) in the process of grassland deterioration (D'Odorico et al., 2013). When a tipping point was unreached, the grassland structures or functions (e.g. vegetation cover, productivity) reduced gradually caused by disturbance that was called grassland degradation (gradual change within a state). At one tipping point, the grassland ecosystem shifted from the grassland state to the desert state that was called grassland desertification (state conversion) (Zhang et al., 2018). The gradual grassland degradation determines the potential desertification areas (Ma et al., 2021). The conversion from vegetated to unvegetated states is the most sensitive and fragile area in drylands (Zhang et al., 2018). They highly determine the direction of the grassland desertification under disturbance. Understanding the dynamics of grassland degradation and desertification separately is therefore of paramount importance to conduct region-precise management and restoration activities (Andrade et al., 2015).

Remote sensing is often used for change detection in grasslands from regional to global scales (Burrell et al., 2017; Burrell et al., 2018; Sahin et al., 2022). For example, the Normalized Difference Vegetation Index (NDVI), as a proxy for ecosystem productivity and vegetation condition (Cetin et al., 2022; Cetin et al., 2021; Degerli and Cetin, 2022; Nama et al., 2022; Pace et al., 2021), was widely used to track land degradation and desertification by trend analysis approaches (Bai et al., 2019; Higginbottom and Symeonakis, 2014; Jabal et al., 2022). The relationships between vegetation indices and climate variables (e.g., precipitation) were another commonly used indicator to measure land conditions (Burrell et al., 2017; Evans and Geerken, 2004). Yet, existing studies usually concentrated on the vegetation dynamics over the whole study region, which hardly separated the grassland degradation and desertification individually and examined the vegetation dynamics within each state explicitly (Jiang et al., 2017; Mariano et al., 2018).

The drivers of grassland degradation and desertification in CA are complicated in spatial scales due to the high sensitivity of vegetation to large climate variations and various human activities (Bardgett et al., 2021; Chen et al., 2020). Although much attention had focused on examining the drivers of land degradation in CA in recent decades, it remains poorly quantified on the contributions of each climate and land use factor to grassland degradation or desertification explicitly at the pixel scale to present the spatial heterogeneity of the drivers (Chen et al., 2020; Jiang et al., 2019; Xu et al., 2016). Additionally, the effects of rising CO<sub>2</sub> on vegetation trends were few considered in the existing

driving force analyses in CA (de Beurs et al., 2015; Zhang et al., 2018; Zhou et al., 2015). Furthermore, the roles of anthropogenic climate change (ACC), including both changes in water availability (driven by variations of precipitation and temperature) and water use efficiency (driven by rising CO<sub>2</sub>), were found significant in land degradation (degraded 5.43 million km<sup>2</sup> of land) of drylands globally (Burrell et al., 2020). However, how ACC affects the grassland dynamics in CA remains unclear (Jiang et al., 2022).

In this study, we aimed to separately analyze the grassland degradation and desertification processes in CA and disentangle the contributions of CO<sub>2</sub> fertilization, climate, land use, and ACC quantitatively at the pixel scale. To achieve these goals, we first identified the different land state regions, including persistent grassland zone (PGZ), desertification zone (DZ), and persistent desert zone (PDZ), by monitoring the annual grasslands and sparsely vegetated lands (consisting of DZ and PDZ) from 2000 to 2020. We then examined the vegetation dynamics over the three state zones during the last two decades, respectively. Finally, we quantified the contributions of rising CO<sub>2</sub>, climate change, climate variation, land use, and ACC on grassland degradation and desertification at the pixel scale. We especially compared the driving factors among different state zones. This study provided an observation-based methodology to carry out refined study on grassland dynamics and the associated drivers at regional to global scales to enhance the stakeholders' knowledge.

## 2. Materials and methods

### 2.1. Study area

Central Asia is in the core region of the Eurasian continent, including five countries of Kazakhstan, Uzbekistan, Turkmenistan, Kyrgyzstan, and Tajikistan, with a total area of about 4 million square kilometers (Fig. 1a). It is dominated by plains and hills having the topography high in the east and low in the west. It has a dry continental climate, characterized by scarce precipitation, high evapotranspiration, and large temperature fluctuations (Zhu et al., 2019). The mean annual precipitation (MAP) is about 270 mm ranging from ~400 mm in the lowlands of the northern part to <100 mm in the southwest areas of Central Asia (Zhou et al., 2015). According to the Moderate Resolution Imaging Spectroradiometer (MODIS) land cover map (MCD12Q1) in 2019, grasslands constitute the largest ecosystem covering about 72% of the total area, followed by barren or sparsely vegetated lands (14.7%) and croplands (5.5%) (Fig. 1a).

### 2.2. Data

#### 2.2.1. Land cover data

The annual 500-m MODIS land cover data (MCD12Q1, Version 6.1) from 2001 to 2019 were collected using the Google Earth Engine platform (Gorelick et al., 2017). This study used the product generated based on the International Geosphere-Biosphere Program (IGBP) classification scheme with 17 land cover classes (Sulla-Menashe et al., 2019).

#### 2.2.2. Land surface reflectance data

The MODIS surface reflectance products with 8-day intervals (MOD09A1) were used to build the long-term vegetation index (VI) time series from 2000 to 2020. The observation quality of the images was estimated at the pixel scale in three steps. First, the bad observations from clouds and cloud shadows were eliminated using the quality assurance layer. Then, the reflectance of the blue band  $\geq 0.2$  was also used as a complementary approach to remove the pixels with cloud contamination. Third, the snow pixels were excluded using the algorithms of normalized difference snow index (NDSI)  $> 0.4$  and NIR  $> 0.11$  (Xiao et al., 2005).

The surface reflectance data with good quality were used to calculate

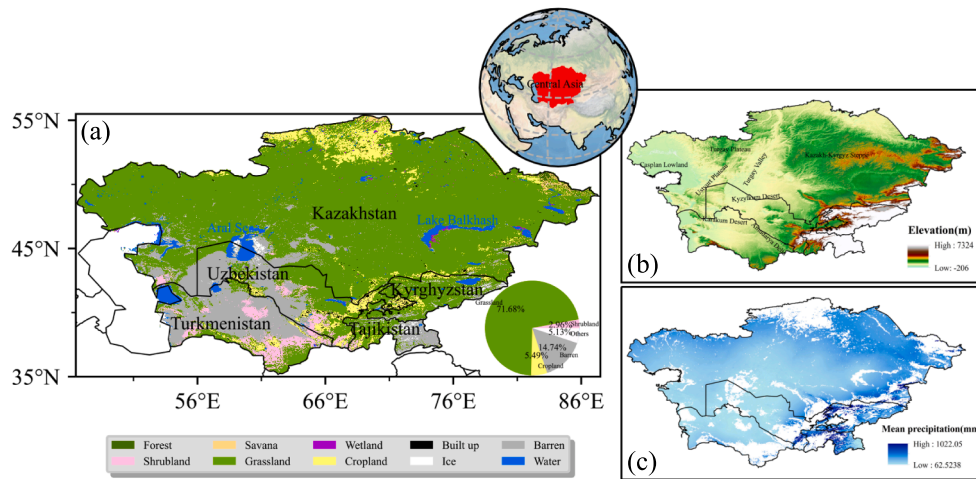


**Fig. 1.** Location of Central Asia (CA). (a) Spatial distribution and proportion of land cover types in CA in 2019 based on MCD12Q1; (b) Topography of CA using the digital elevation model (DEM); (c) Distribution of the annual mean precipitation during 2000–2020.

the Enhanced Vegetation Index (EVI) (Huete et al., 2002), Land Surface Water Index (LSWI) (Xiao et al., 2005), and NDSI (Hall et al., 2002). EVI was used considering its higher robustness to the interference of atmosphere and soils than NDVI (Huete et al., 2002). LSWI was sensitive to leaf and soil water (Xiao et al., 2006). The gaps in the VI time series resulting from the quality control were filled using the linear interpolation approach.

$$NDSI = \frac{\rho_{Green} - \rho_{SWIR}}{\rho_{Green} + \rho_{SWIR}} \quad (1)$$

$$EVI = 2.5 \times \frac{\rho_{NIR} - \rho_{Red}}{\rho_{NIR} + 6 \times \rho_{Red} - 7.5 \times \rho_{Blue} + 1} \quad (2)$$

$$LSWI = \frac{\rho_{NIR} - \rho_{SWIR}}{\rho_{NIR} + \rho_{SWIR}} \quad (3)$$

where  $\rho_{Blue}, \rho_{Green}, \rho_{Red}, \rho_{NIR}$  and  $\rho_{SWIR}$  are the surface reflectance values of blue, green, red, near-infrared, and shortwave-infrared bands.

### 2.2.3. Land surface temperature (LST) data

LST is a critical variable to understand land–atmosphere interactions (Kumar et al., 2022). A range of satellite sensors (such as ASTER, Landsat, and MODIS) can provide LST information over the Earth’s surface (Cetin, 2019). We collected the MODIS LST products from Terra (MOD11A2, Version 6.1) for the years 2000 to 2020, which have an 8-day temporal interval and 1-km spatial resolution. MOD11A2 datasets provide daytime and nighttime LST at ~10:30 am and ~10:30 pm local solar time, respectively. In this study, the thermal growing season (TGS) was calculated using the nighttime LST. It was reported that this LST product had an absolute error of <1 K (Wan, 2014). The valid pixels with the quality flag as ‘00’ or ‘01’ in the quality layer were used in this study. The linear interpolation approach was used to fill the gaps in the LST time series. The TGS was defined based on the LST following the fact that plant growth needs the temperature reach to a threshold. The start and end of the LST-based growing season were calculated with nighttime LST above 0 °C (LST0) for continuous three 8-d intervals in each year from 2000 to 2020. To match the spatial resolution of MOD09A1, the resultant maps of the start and end dates were resampled into 500 m using the nearest neighbor interpolation method.

### 2.2.4. Climate datasets

The climate variables of air temperature, precipitation, and CO<sub>2</sub> were used to examine the driving factors of vegetation dynamics in Central Asia. The information on air temperature and precipitation was

obtained from the TerraClimate dataset from 2000 to 2020. The TerraClimate provides monthly climate variables and water balance for global terrestrial surfaces. It was generated by using climatically aided interpolation, combining high-spatial-resolution, but time-varying data from CRU Ts4.0 and the Japanese 55-year Reanalysis (JRA55) (Abatzoglou et al., 2018). Conceptually, the procedure applies interpolated time-varying anomalies from CRU Ts4.0/JRA55 to the high-spatial-resolution dataset that covers a broader temporal record (Abatzoglou et al., 2018). The dataset was obtained from the Google Earth Engine platform. The global CO<sub>2</sub> concentration was obtained from the Intergovernmental Panel on Climate Change (IPCC) historical forcing data (Meinshausen et al., 2011).

## 2.3. Methods

To understand the dynamics and driving factors of grassland degradation and desertification in Central Asia in the last two decades (2000–2020), we developed a workflow that includes three major study sections (Fig. 2). First, we generated the annual vegetated and sparsely vegetated land during 2000 to 2020, which were used to identify the PGZ, DZ, and PDZ using the frequency analysis method. Second, we analyzed the vegetation dynamics over the vegetated zones of PGZ, DZ, and PDZ using trend analysis methods. Third, we quantified the contributions of potential driving factors (including climate and human activity) to grassland deterioration across the three state zones. The methods of each section were introduced in detail in the following text.

### 2.3.1. Extraction of the targeted area

This study focused on grassland degradation and desertification in Central Asia, which covered a targeted study area that included three land cover types, i.e., grasslands, barren or sparsely vegetated regions, and desert regions. We first used the IGBP-based MODIS land cover products (MCD12Q1) to extract the annual distribution of grasslands and barren or sparsely vegetated lands for the period of 2001 to 2019. Second, additional masks, including the water body, croplands, forests, and wetlands, were applied to reduce the uncertainties of the annual maps from MCD12Q1. According to our previous algorithms (Zhang et al., 2018), the water body pixels can be identified by the maximum EVI lower or equal to zero during the TGS within a year. The croplands, forests, and wetlands pixels had LSWI values >0 at least last for ten 8-day composites during the TGS within a year. Finally, we extracted the targeted area with the potential for grassland degradation and desertification by intersecting the annual IGBP-based maps of grasslands, and barren or sparsely vegetated lands from 2001 to 2019. Thus,

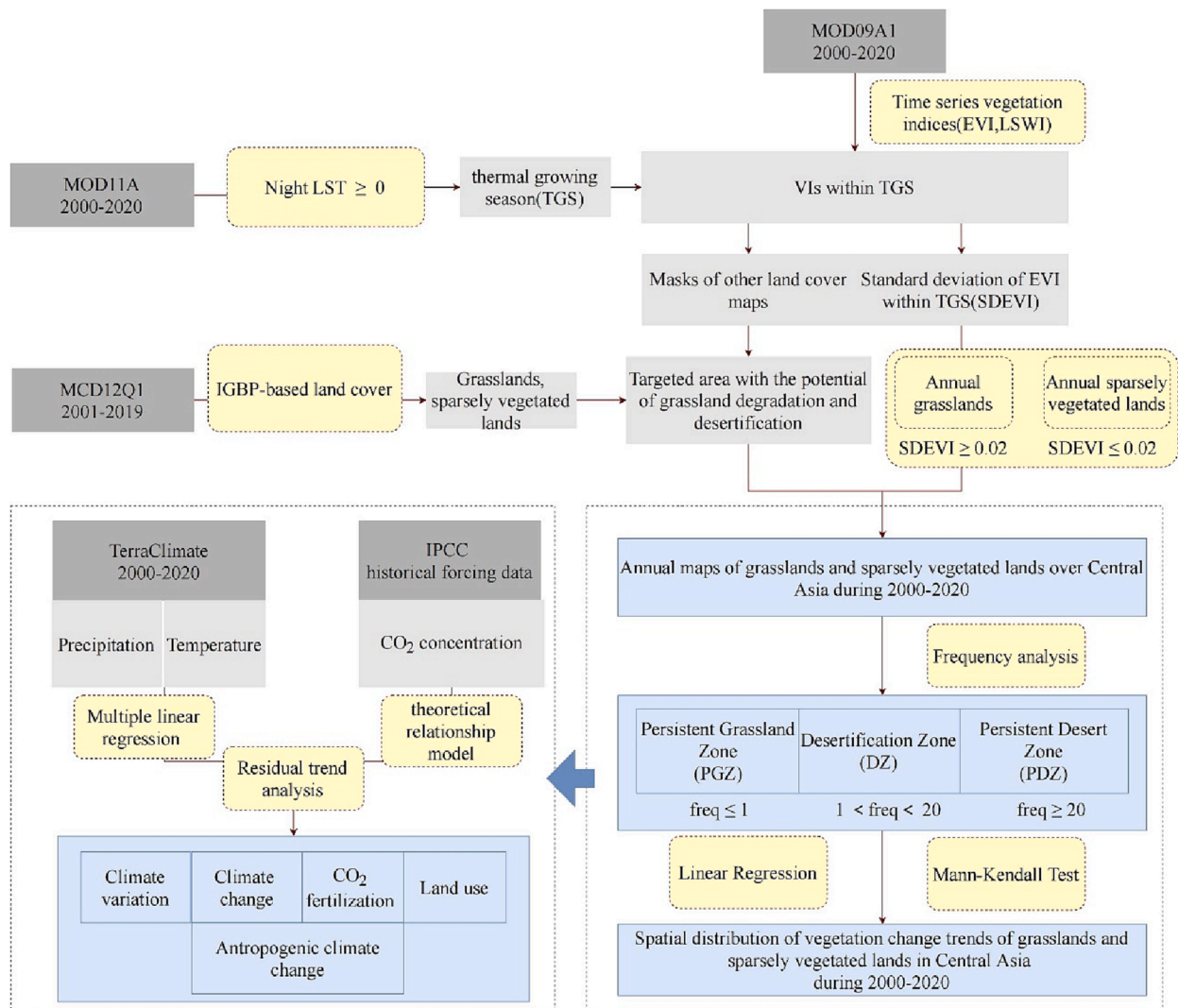


Fig. 2. The workflow of this study.

the targeted area allowed us to focus only on those changes between grasslands and sparsely vegetated regions.

### 2.3.2. Separation of grasslands and sparsely vegetated lands

To determine the ecosystem states for each year during 2000–2020 in the bi-stable theory frame (D’Odorico et al., 2013), we reclassified the targeted area as grasslands and sparsely vegetated lands. These two land cover types had significant differences in vegetation coverage, which resulted in the different seasonal dynamics of the land surface. This seasonal feature can be detected by the variation of EVI in the TGS, which was a stable variable to separate the sparsely vegetated lands and grasslands (Zhang et al., 2018). Thus, within the TGS, we calculated the standard deviation (SD) of EVI as an indicator to map the annual grasslands and sparsely vegetated lands. This indicator was denoted as SDEVI<sub>TGS</sub> in this study. Specifically, to determine the thresholds of classification, we analyzed the frequency distributions of SDEVI<sub>TGS</sub> for each vegetation type based on ~10,000 random samples obtained from every year of 2001–2019 (500 samples for each year) (Fig. S1a). It showed that the SDEVI<sub>TGS</sub> for the barren or sparsely vegetated lands was low, which can be separated by a threshold of 0.02 from grasslands (Fig. S1b). Thus, the grasslands and sparsely vegetated lands were classified by an algorithm of SDEVI<sub>TGS</sub> > 0.02 in this study. Here, the sparsely vegetated lands refer to the regions with vegetation coverage of <10%.

### 2.3.3. Mapping different state zones of PGZ, DZ, and PDZ

According to the bi-stable desertification theory (D’Odorico et al., 2013), the targeted area consisted of single stable systems of grasslands (PGZ) and deserts (PDZ), and two state conversion regions (DZ) in this study. These three-state zones were identified by using a frequency analysis approach based on the annual maps of grasslands and sparsely vegetated lands during 2000–2020. According to the number of years for the pixel covered by grasslands or sparsely vegetated lands during 2000–2020, pixels were classified as PGZ, DZ, and PDZ with sparsely vegetated lands covered for 0–1 year (never or rarely), 2–19 years (sometimes), and 20–21 years (usually or always), respectively.

### 2.3.4. Analyses of vegetation trends among different state zones

To assess the vegetation dynamics within the state zones of PGZ, DZ, and PDZ, we analyzed the long-term EVI trends during 2000–2020. The temporal trends of mean EVI during the thermal growing season (EVI<sub>TGS</sub>) were examined by two approaches, including the linear regression and the Mann-Kendall test (McLeod, 2005). The slopes of the linear least squares regression and Mann-Kendall test were used to evaluate the temporal trends in the study period. The statistical significances of EVI<sub>TGS</sub> temporal trends were estimated at the pixel and different state zone scales, respectively.

### 2.3.5. Detection of drivers for grassland degradation and desertification

In this study, we quantified the impacts of the CO<sub>2</sub> fertilization effect, climate change (CC), climate variability (CV), land use, and other factors on the vegetation change in the targeted area during 2000–2020 by an observation-based approach (Burrell et al., 2020). We used EVI<sub>TGS</sub> as a proxy of vegetation growth to calculate the vegetation change in the targeted area (Eq. (4)).

$$\Delta EVI_{TGS} = slope \times (Y_{end} - Y_{start}) \quad (4)$$

where *slope* was the result of the Theil-Sen slope estimator.  $Y_{start}$  and  $Y_{end}$  were the start and end years of the time series. The overall vegetation change ( $\Delta EVI_{obs}$ ) was quantified using Eq. (4) with the observed EVI<sub>TGS</sub> time series from 2000 to 2020.

To quantify the CO<sub>2</sub> fertilization effect on vegetation change, we followed the theoretical model to indicate the relationship between plant productivity and increasing CO<sub>2</sub> (Eq. (5)) (Burrell et al., 2020). Then we applied the relationship to EVI<sub>TGS</sub> data (EVI<sub>obs</sub>) to generate the EVI<sub>TGS</sub> estimate (EVI<sub>adj</sub>) that excluded the CO<sub>2</sub> effect using Eq. (6) (Burrell et al., 2020).

$$GPP_{rel} \approx \frac{(c_a - \Gamma^*)(c_{a0} + 2\Gamma^*)}{(c_a + 2\Gamma^*)(c_{a0} - \Gamma^*)} \quad (5)$$

where  $GPP_{rel}$  was the relative CO<sub>2</sub> assimilation rate (%),  $c_a$  was the atmospheric CO<sub>2</sub> concentration ( $\mu\text{mol}/\text{mol}$ ),  $\Gamma^*$  was the CO<sub>2</sub> compensation point in the absence of dark respiration ( $\mu\text{mol}/\text{mol}$ ),  $c_{a0}$  was the CO<sub>2</sub> concentration in the start year of the time series,  $\Gamma^* = 40$  ( $\mu\text{mol}/\text{mol}$ ).

$$\frac{EVI_{obs}}{EVI_{adj}} \approx \frac{NPP_{obs}}{NPP_{base}} \approx GPP_{rel} \quad (6)$$

where  $NPP_{obs}$  was the NPP at the observed atmospheric CO<sub>2</sub> concentration ( $c_a$ ),  $NPP_{base}$  was the NPP given the same climate conditions but an atmospheric CO<sub>2</sub> concentration of  $c_{a0}$ . The vegetation change attributed to the increasing CO<sub>2</sub> ( $\Delta EVI_{CO_2}$ ) can be calculated by Eq. (4) with the (EVI<sub>obs</sub> - EVI<sub>adj</sub>) time series.

To quantify the effects of land use (LU) on vegetation change, we used multiple linear regression methods with EVI<sub>adj</sub> and the climate factors (precipitation and temperature) to build a Vegetation Climate Relationship (VCR) (Burrell et al., 2020). RESTREND was applied to calculate the vegetation change caused by LU ( $\Delta EVI_{LU}$ ) by calculating the residuals of the VCR and EVI<sub>adj</sub>.

The climate effects on EVI<sub>TGS</sub> (EVI<sub>CL</sub>) were separated into CC in a long period (EVI<sub>CC</sub>) and interannual CV (EVI<sub>CV</sub>). Based on the per-pixel VCR, the EVI<sub>CL</sub> and EVI<sub>CV</sub> were calculated using the observed climate data and the detrended climate data, respectively (Burrell et al., 2020). The difference between EVI<sub>CL</sub> and EVI<sub>CV</sub> was attributed to CC (EVI<sub>CC</sub>). Thus, the EVI<sub>TGS</sub> changes can be attributed to CC and CV ( $\Delta EVI_{CC}$ ,  $\Delta EVI_{CV}$ ). The contribution of other factors (OF) on EVI<sub>TGS</sub> was calculated as Eq. (7).

$$\Delta EVI_{OF} = \Delta EVI_{obs} - \Delta EVI_{CO_2} - \Delta EVI_{LU} - \Delta EVI_{CC} - \Delta EVI_{CV} \quad (7)$$

Finally, the effect of ACC was calculated as the sum of CO<sub>2</sub> and CC, due to it being linked to the changes in water availability driven by the long-term trends of precipitation and temperature and the changes in water use efficiency caused by rising CO<sub>2</sub>.

## 3. Results

### 3.1. Annual maps of grasslands and sparsely vegetated lands in CA from 2000 to 2020

We generated the annual maps of grasslands and sparsely vegetated lands in Central Asia from 2000 to 2020 based on land cover classification data and additional masks. We compared the resultant annual grassland maps with five national-scale land cover datasets at different

spatial resolutions (Supplementary method 1, Fig. S2). The comparison showed our results were consistent with other products with slopes ranging from 0.94 to 1.28 and  $R^2$  of 0.99. Therefore, it is reasonable to analyze the grassland degradation and desertification over the past two decades at the annual interval based on our resultant maps.

The grasslands in Central Asia are mainly distributed in central Kazakhstan, bordering on the sparsely vegetated lands in southern Kazakhstan and north central Uzbekistan (Fig. 3). In terms of temporal dynamics, the area of grasslands reached the largest in 2016, followed by 2002 and 2019, while that in 2008 was the lowest (Fig. 4a). Compared with 2000, the grassland area in 2020 only decreased by 2.32% and no obvious decreasing trend ( $P > 0.1$ ) was observed (Fig. 4a). In terms of the spatial dynamics of the sparsely vegetated lands, it showed that desertification expanded northward that directly threatened the northern grasslands (Fig. 4b). However, the grassland desertification was alleviated in recent years (after 2014).

### 3.2. Recognition of three desertification state zones

According to the pixel-scale frequency analysis on sparsely vegetated lands that occurred from 2000 to 2020, the targeted area was classed as PGZ, DZ, and PDZ (Fig. 5a). The PGZ, DZ, and PDZ were distributed from north to south in Central Asia, and PGZ and DZ presented strip distribution from west to east. DZ dominated the region with an area proportion of 44.76%, followed by PGZ accounting for 38.74%. The area of PDZ was the smallest only having a ratio of 16.50%, which was mainly distributed in Turkmenistan and Uzbekistan (Fig. 5a). DZ was a transitional zone between PGZ and PDZ that was a key hotspot to desertification in CA. This fragile ecotone determined the direction of grassland desertification and restoration. Between 2000 and 2020, the conversion frequency between grasslands and sparse vegetation lands was assessed, which showed the vulnerability for desertification in DZ (Fig. 5b).

### 3.3. Vegetation changes in different state zones

We analyzed the vegetation changes at the regional and pixel scales. At the regional scale, we examined the linear trend of the annual EVI<sub>TGS</sub> over the entire targeted area and three state zones (PGZ, DZ, PDZ) (Fig. 6c). From 2000 to 2020, the annual EVI<sub>TGS</sub> fluctuated in the whole region without an obvious trend ( $P > 0.1$ ,  $n = 21$ ). Considering the different state zones, the greenness of DZ and PDZ presented increasing trends (slope  $> 0$ ), whereas that of PGZ showed a slightly decreasing trend (slope  $< 0$ ) despite insignificant signals ( $P > 0.1$ ). As a result, this indicated that the grassland desertification in CA was improving, while the grassland degradation here continued.

At the pixel scale, the annual EVI<sub>TGS</sub> trends were calculated by the linear regression and Mann-Kendall methods. According to the linear regression results (Fig. 6a), most regions in Central Asia showed a greening trend of EVI<sub>TGS</sub> (63%), which was near twice the area of the browning trend. Specifically, the significant increasing trend was 12% and 18% for the targeted area at significance levels of  $P < 0.05$  and  $P < 0.1$ , respectively. Most significant increases in EVI<sub>TGS</sub> mainly occurred in the east-central part of Kazakhstan, which was mostly in the zone of DZ. In terms of the proportions of each state zone in the greening and browning trends (Fig. 6d), DZ dominated the greening regions accounting for 45% and 46% at significance levels of  $P < 0.05$  and  $P < 0.1$ , followed by PDZ (~35%) and PGZ (~20%). However, the significant browning trends largely concentrated in the PGZ accounting for ~66% ( $P < 0.05$  and  $P < 0.1$ ), which was much higher than the proportions of DZ (~28%) and PDZ (~6%). The results showed the grassland degradation in CA was exacerbated from 2000 to 2020 and mainly distributed in western Kazakhstan. Similar results were shown in the Mann-Kendall test (Fig. 6b). Detailed statistical information was shown in Table S1.

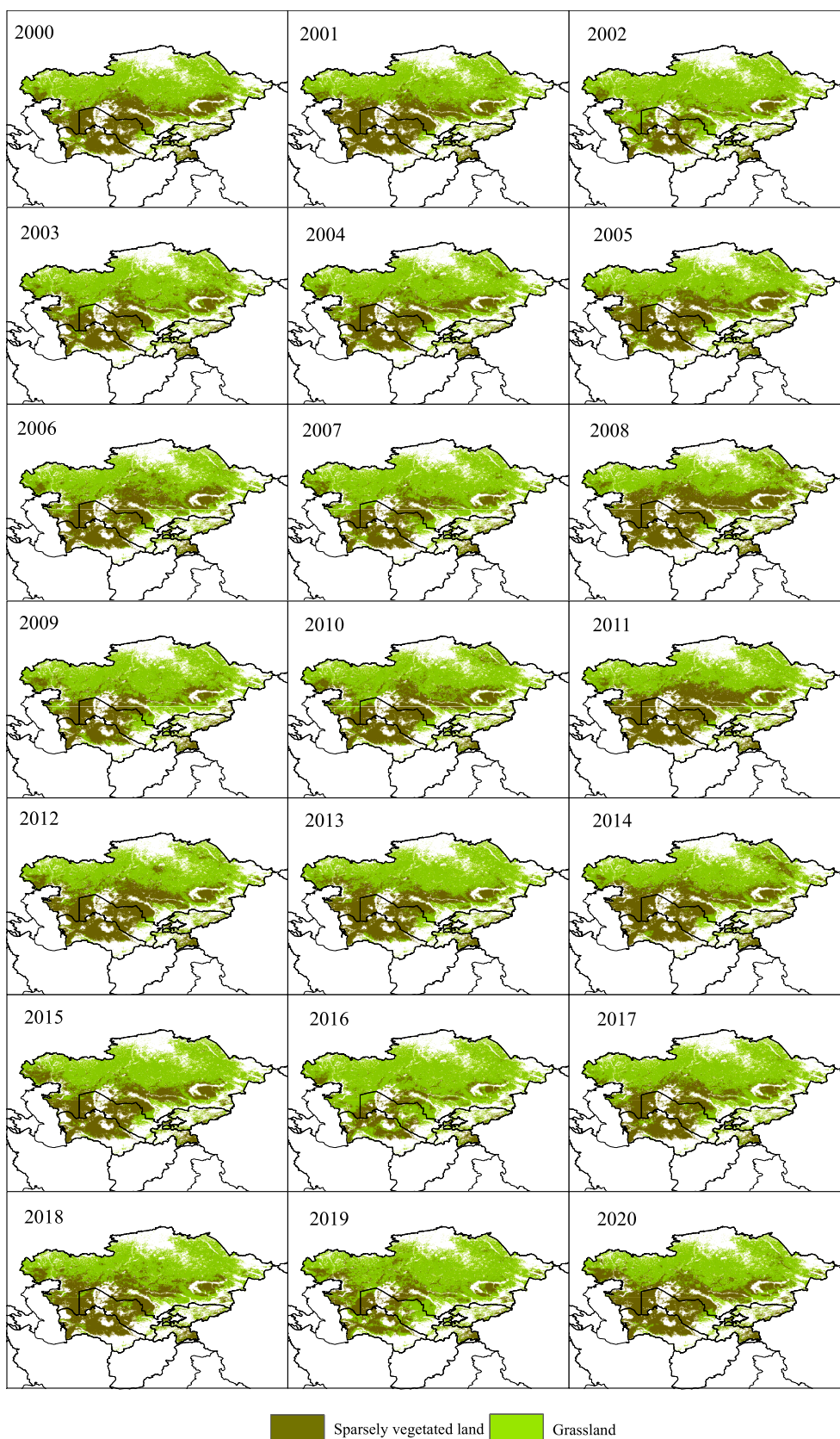
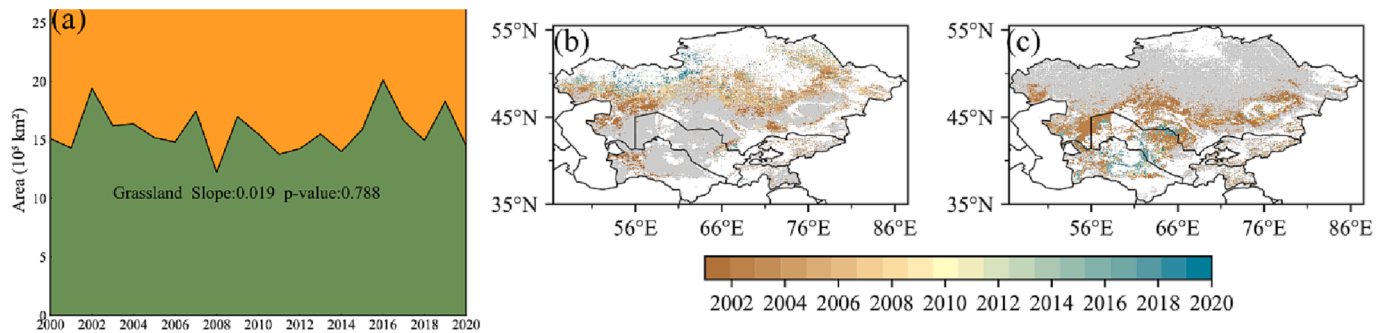
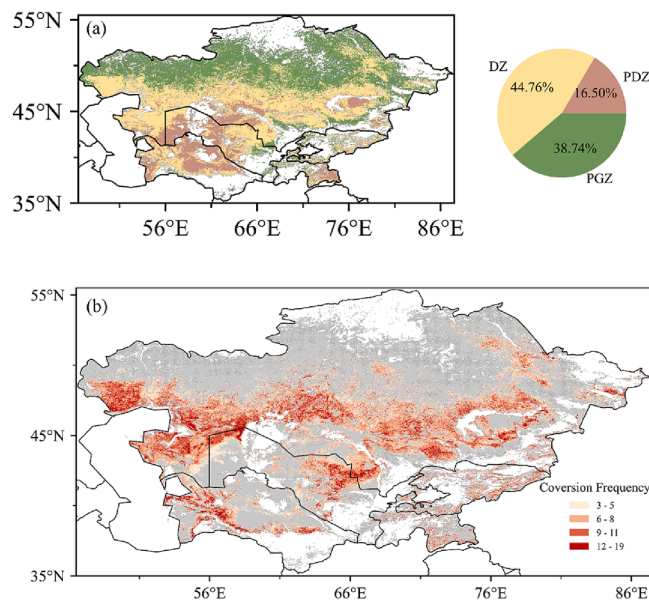


Fig. 3. The annual distributions of grasslands and sparsely vegetated lands in Central Asia during 2000–2020.



**Fig. 4.** Grassland area dynamics in Central Asia. (a) Area of grasslands during 2000–2020; (b) The first year of conversion from grasslands to barren or sparsely vegetated lands during 2000–2020 (barren or sparsely vegetated lands in 2000 was colored as gray); (c) The first year of conversion from barren or sparsely vegetated lands to grasslands (grasslands in 2000 was colored as gray).



**Fig. 5.** (a) Spatial distributions of three state zones in Central Asia, including the permanent grassland zone (PGZ), desertification zone (DZ), and permanent desert zone (PDZ). (b) The conversion frequency between grasslands and sparsely vegetated lands in DZ during 2000–2020.

### 3.4. Impacts of different factors on vegetation changes

The processes of grassland degradation and desertification are closely related to human activities and environmental factors. Throughout the targeted area, the area of vegetation changes mainly affected by LU accounted for the largest proportion (46%), followed by rising  $\text{CO}_2$  (26%), CC (20%), and then CV (4%) (Fig. 7b). Land use was a driving factor that cannot be ignored in any region. In addition, from PGZ, DZ to PDZ, the proportion of the area affected by the rising  $\text{CO}_2$  increased gradually (Fig. 7b). Although CC was not the main driving factor in PGZ, DZ, and PDZ, it had a very important impact on the browning region (Fig. 7b).

The effects of individual driving factors, including  $\text{CO}_2$ , LU, CC, and CV, on vegetation dynamics were showed in Fig. 8a–d at the pixel scale. The mean contributions of each factor were then summarized at different subdivisions (Fig. 8f). Vegetation degradation in PGZ mainly resulted from the negative impacts of CC and CV. The alleviation of grassland desertification in DZ and PDZ resulted from the positive impacts of LU and rising  $\text{CO}_2$ . LU played a key role in vegetation change. In addition, CC and CV mainly contributed to vegetation degradation. The  $\text{CO}_2$  fertilization effect in PGZ was stronger than those in DZ and PDZ, but it could not reverse the vegetation degradation caused by climatic

factors. ACC had a positive effect over the study periods in general. Despite widely positive effects, ACC also had a decreasing effect across 20.63% of the target area, mainly distributed in west Kazakhstan and Uzbekistan (Fig. 8e). In most of the targeted area, the negative effects of LU were offset by the positive effects of ACC (Fig. 8b).

## 4. Discussion

### 4.1. The dynamics of grassland degradation and desertification in CA

Grassland degradation and desertification refer to two processes including the vegetation change within one state and the conversion between vegetation and non-vegetation states (D'Odorico et al., 2013). Due to different conservation and restoration approaches adopted for different land states, accurate spatial information on the land states was helpful to support effective mitigation strategies, especially for the drylands with vulnerable land cover types (Yao et al., 2020). Previous studies focused on the trends of vegetation greenness or production to examine the combined phenomena of grassland degradation and desertification in CA, but the different states were not separated clearly (Chen et al., 2020; Jiang et al., 2017). Therefore, this study used a two-step approach: firstly, to identify the state zones of PGZ, DZ, and PDZ in the study area, respectively (Fig. 5b), and then to examine the  $\text{EVI}_{\text{TGS}}$  trends to describe the grassland degradation and restoration in different state zones (Fig. 6). This approach was developed in our previous study, which found the sparsely vegetated area was increasing with exacerbated desertification during 2000 to 2014 (Zhang et al., 2018). Yet this study showed the sparsely vegetated area slightly decreased after 2014, which showed a neutral trend from 2000 to 2020 (Fig. 4a). As the start and end conditions affected the results of grassland dynamic trends in drylands, the different study periods between these two works could explain the discrepancy in the findings (Burrell et al., 2020; Fensholt et al., 2012). Our results on the dynamics of the  $\text{EVI}_{\text{TGS}}$  in CA were also supported by a recent study (Jiang et al., 2022). The study also observed a decreasing trend of land degradation in the period of 2015–2019 with 2015 as one of the main abrupt-change years in the time series analyses on land degradation from 2000 to 2019 in CA. In addition, the year 2008 was also reported as an abrupt year caused by severe drought in other works (Xu et al., 2016; Zhu et al., 2019).

Our study underlined more attention should be paid to the grassland degradation over the PGZ (Fig. 5b). As shown in the results, the area of grasslands was almost stable or slightly decreasing despite obvious interannual variations from 2000 to 2020. However, the trends of land surface browning mainly happened in the PGZ, while the greening trends were more obvious in the DZ and PDZ (Fig. 6d). The evident browning trends over the grasslands in the north of Kazakhstan were also reported in other studies covering different time windows, such as 2000–2014 (Zhang et al., 2018), 2000–2019 (Jiang et al., 2022), 1998–2013 (Li et al., 2015), 1990–2009 (Mohammad et al., 2013). The

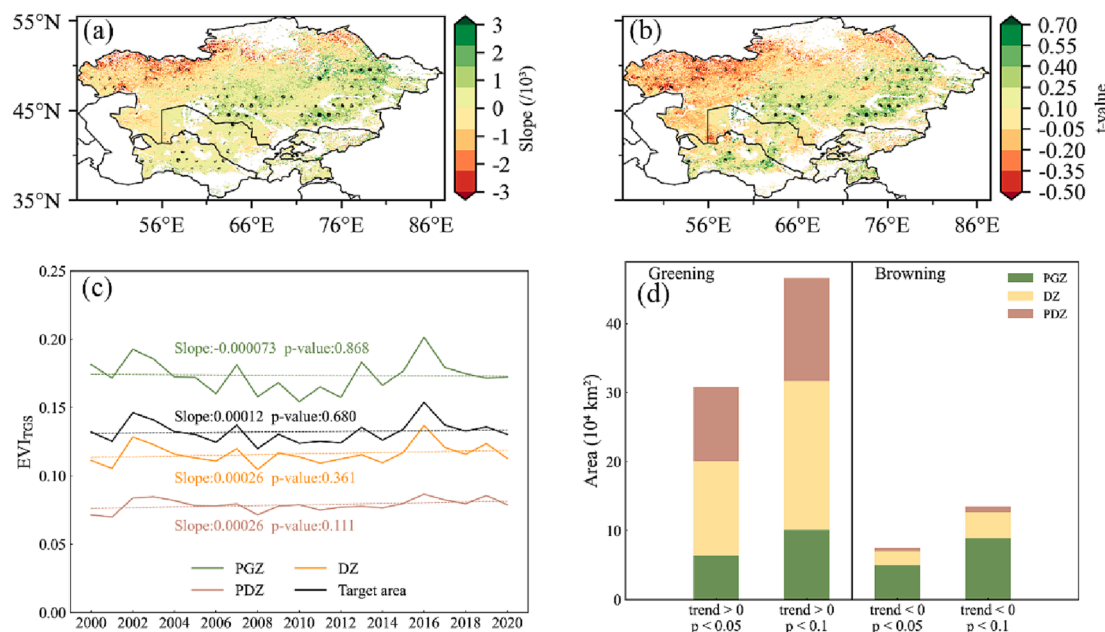


**Fig. 6.** Spatial-temporal dynamics of annual mean EVI in the growing season (EVI<sub>TGS</sub>) during 2000–2020. (a) Linear regression trend and (b) Mann Kendall trend of EVI<sub>TGS</sub> in the target area of Central Asia during 2000–2020. The t-value was Kendall's tau coefficient. Plus symbols in Fig. a, b denote statistically significant trends at 0.1 level; (c) Trends of averaged EVI<sub>TGS</sub> in different state zones, i.e., permanent grassland zone (PGZ), desertification zone (DZ) and permanent desert zone (PDZ); (d) The area statistics of different state zones for the significant greening (trend > 0, p < 0.05; trend > 0, p < 0.1) and browning regions (trend < 0, p < 0.05; trend < 0, p < 0.1).

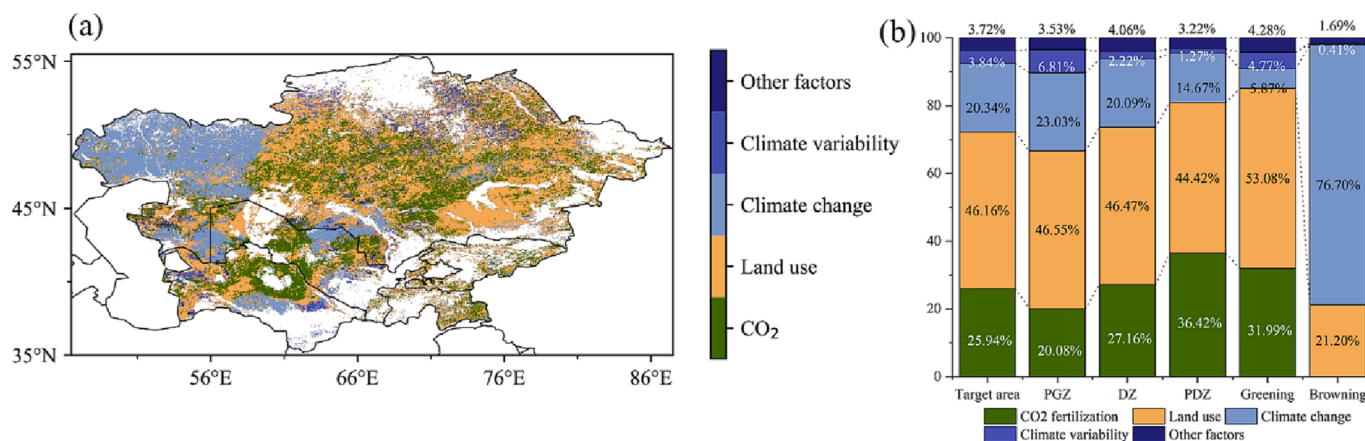


**Fig. 7.** (a) Spatial distributions of the main driving factors on the annual dynamics of EVI in the growing season in Central Asia (CA). The main driving factors included rising CO<sub>2</sub>, land use, climate change, climate variability, and other factors. (b) The area proportions of different driving factors for individual subdivisions of CA, including the whole targeted area, permanent grassland zone (PGZ), desertification zone (DZ) and permanent desert zone (PDZ), greening and browning regions.

significant greening trends mainly occurred in the sparsely vegetated region, especially in eastern Kazakhstan (Fig. 6), which agreed well with the previous results (Chen et al., 2019; Jiang et al., 2022; Jiang et al., 2019). Due to the grasslands in these regions being sensitive to precipitation, some sparsely vegetated regions have transferred to grasslands with increased precipitation that led to the desertification reversion in southern Kazakhstan and mountain regions (Jiang et al., 2019). These results agreed with the widely greening trends over global drylands in the past thirty years observed by satellites (Wang et al., 2022). Yet, our study pointed out that although the total area of grasslands may be stable for the study period, the degradation in PGZ would potentially increase the DZ or PDZ in the future. This study provided observation evidence for the simulation results, which revealed that the area of desert lands decreased during 1980–2015, but the area of potential desert lands increased in CA (Ma et al., 2021).

#### 4.2. The drivers of grassland degradation and desertification in CA

The drivers of grassland degradation and desertification in CA have been widely examined in previous studies (Chen et al., 2019; Chen et al., 2020; Jiang et al., 2022; Yuan et al., 2021; Zhou et al., 2019). However, these studies mainly concentrated on the climate variables of temperature, precipitation, drought, and human activities (Chen et al., 2019). It was lacking to consider the roles of CO<sub>2</sub> and ACC on grassland degradation and desertification. Our study systematically quantified the drivers of rising CO<sub>2</sub>, CC, CV, LU, and ACC for grassland degradation and desertification in CA at the pixel scale (Fig. 8). The results demonstrated that rising CO<sub>2</sub> was the largest driver of vegetation greening over the whole targeted area and subdivision regions. This result supported the findings that rising CO<sub>2</sub> was a driver of global dryland greening, as elevated CO<sub>2</sub> can relieve the water stress for plant growth within the drying atmosphere in drylands (Lian et al., 2021; Lu et al., 2016).

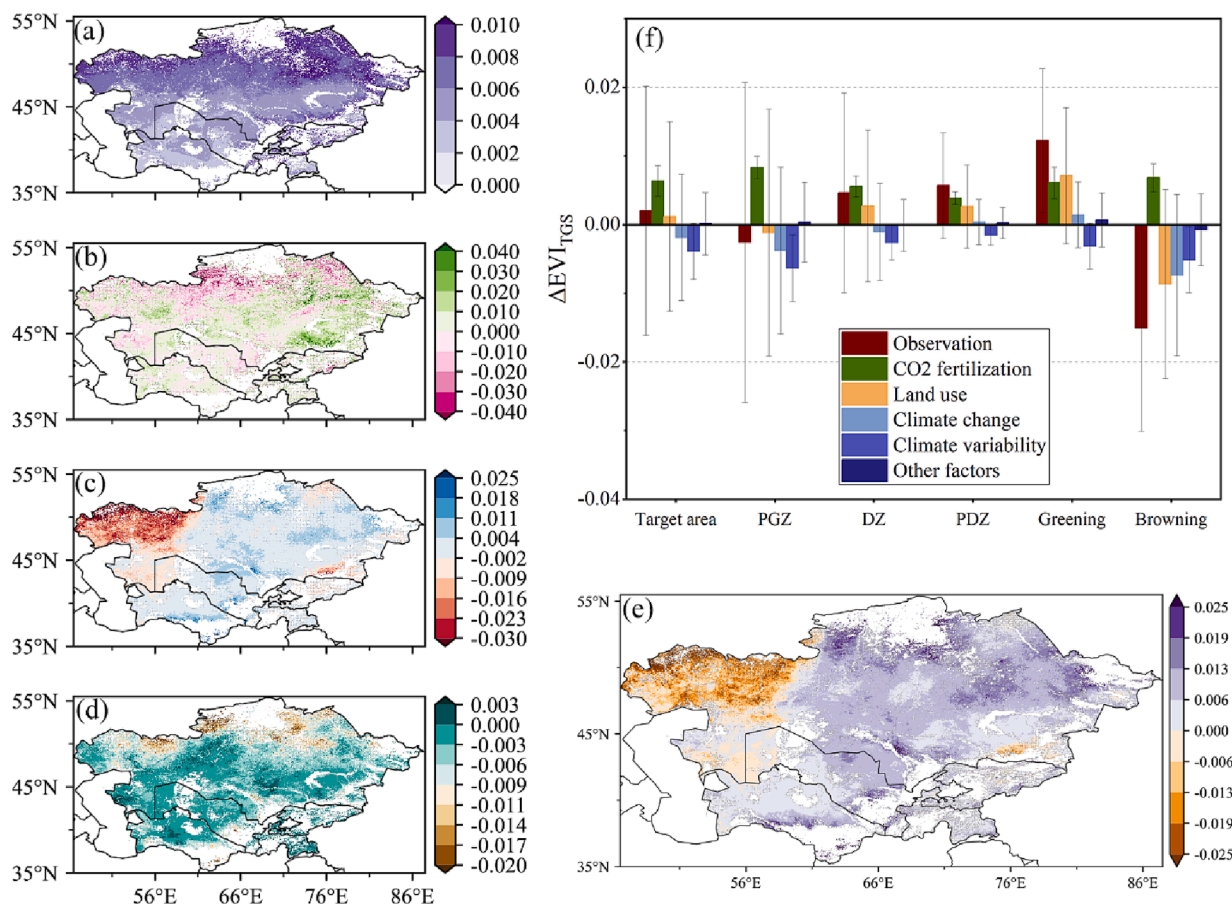


**Fig. 8.** Contributions of individual driving factors to the changes in  $\text{EVI}_{\text{TGS}}$  between 2000 and 2020 were quantified at the pixel scale. The driving factors included (a) CO<sub>2</sub> fertilization, (b) land use (LU), (c) climate change (CC), (d) climate variability (CV), and (e) anthropogenic climate change (ACC), respectively; (f) the mean effects of different factors estimated in different subdivisions, including the whole targeted area, permanent grassland zone (PGZ), desertification zone (DZ) and permanent desert zone (PDZ), greening and browning regions.

However, CC and CV mainly presented negative roles on the  $\text{EVI}_{\text{TGS}}$  changes in the study period, particularly CV having the largest negative impacts over the whole targeted area. Long-term temperature increase and drought could cause vegetation degradation dramatically in Eurasian temperate ecosystems not only in CA (de Beurs et al., 2015; Zhang et al., 2018; Zhu et al., 2019). Water availability played a critical role in vegetation growth in grasslands and sparsely vegetated lands (Jiang et al., 2022; Li et al., 2015). Extensive vegetation degradation has been caused by the inter- and intra-annual variations of precipitation and potential evapotranspiration in CA (Jiang et al., 2017; Xu et al., 2016). This study showed that the CV had smaller effects on vegetation change in the PDZ and DZ compared to the PGZ. This result supported the finding that vegetation in drier regions had lower sensitivities to climate variability (Yuan et al., 2021). The effects of ACC combining rising CO<sub>2</sub> and CC presented positive signals on the  $\text{EVI}_{\text{TGS}}$  dynamics in 2000 to 2020 across a wide region (Fig. 8e). The wide positive contributions were consistent with the results of a global desertification study using annual NDVI<sub>max</sub> from 1982 to 2015 (Burrell et al., 2020). But the negative contributions to the northwest PGZ were slightly different, which could be caused by the different study periods and vegetation indices.

Furthermore, LU was shown as a positive driver of land surface greening in CA, especially in DZ and PDZ. A recent study reported that >70% of land improvement in CA came from anthropogenic activities such as irrigation and grassland reclamation (Jiang et al., 2022). In the PGZ, LU showed negative impacts on grassland vegetation. Similarly, previous studies found that human activities, such as increasing livestock, were the main driving factor of the net primary productivity

(NPP) reduction for the grasslands in CA (Chen et al., 2019; Chen et al., 2020). In addition, the spatial heterogeneity of the effects from different drivers in this study was consistent with previous reports (Fig. 7b). We find negative effects of CC and LU in west Kazakhstan, which was consistent with the findings on the drivers in the Ustyurt Plateau and the Atyrau region respectively (Jiang et al., 2017). The shrink of the Aral Sea and the adjacent land degradation resulted from the expansion of croplands in the Amudarya Delta, which agreed with our results (Jiang et al., 2022). Our findings showed that LU played positive effects on vegetation changes around Balkhash Lake, which was supported by the fact that an increase in runoff improved the dryland ecosystems around Balkhash Lake (Duan et al., 2020). Although the positive effect of CO<sub>2</sub> fertilization was stronger in PGZ than that in DZ and PDZ, the different effects of LU, CC, and CV caused the divergent trends between grassland degradation and grassland desertification in the CA.

#### 4.3. Implications and improvements

This study considered grasslands and deserts as bi-stable ecosystems. The transition state from grasslands to deserts was identified as grassland desertification. The reduction of vegetation greenness (i.e., decreasing trends of  $\text{EVI}_{\text{TGS}}$ ) within the grasslands was detected as grassland degradation. This methodology identified more details regarding grassland degradation and desertification over different regions than previous studies. The results supported the development of smart mitigation strategies considering regional variations for achieving zero net land degradation in Sustainable Development Goal 15.3 (Jiang et al., 2022; Yao et al., 2020). Due to the global datasets (e.g., climate,

land cover, vegetation indices) were used in this study, it was possible to apply this methodology into other regions of the world. However, the performance of the method may be affected by the data quality such as data loss. In addition, variations in geographical factors such as elevation, solar radiation, and the length of daytime often lead to the differences of vegetation sensitivity to climate. Therefore, the detection of the grassland growing season in different regions should be adjusted appropriately not only rely on nighttime LST.

As grassland degradation was characterized as the regions with greenness reduction, we did not include the degradation processes that may have increased greenness such as woody plant encroachment or species invasion (Burrell et al., 2020; Venter et al., 2018). Woody plant encroachment has widely happened on the global grasslands (Stevens et al., 2017; Wang et al., 2018a). This phenomenon was also reported in CA and other drylands (Li et al., 2015; Petrie et al., 2015; Wang et al., 2018b). The grassland degradation caused by woody plant encroachment or plant invasion will be examined specially in the future works based on our previous studies (Wang et al., 2017; Wang et al., 2018a).

## 5. Conclusions

This study separated and examined the processes of grassland degradation and desertification in detail, and quantified the roles of different driving factors at the pixel scale. We found that grassland desertification in CA alleviated after 2014, while grassland degradation remained a severe issue that could increase the desertification potential. Although CO<sub>2</sub> fertilization caused vegetation greening widely, the different effects of LU, CC, and CV resulted in the divergent trends between grassland degradation and grassland desertification in CA. The proposed methodology can be implemented into other regions. The results provided some insights into developing region-precise strategies for grassland conservation in CA and other drylands.

## CRedit authorship contribution statement

**Yanbo Zhao:** Methodology, Visualization, Data curation, Formal analysis, Writing – original draft. **Jie Wang:** Methodology, Conceptualization, Supervision, Writing – review & editing. **Geli Zhang:** Methodology, Conceptualization, Supervision, Writing – review & editing. **Luo Liu:** Methodology, Data curation. **Jilin Yang:** Data curation, Formal analysis, Writing – review & editing. **Xiaocui Wu:** Data curation, Formal analysis, Writing – review & editing. **Chandrashekar Biradar:** Methodology, Conceptualization, Supervision, Writing – review & editing. **Jinwei Dong:** Methodology, Conceptualization, Supervision, Writing – review & editing. **Xiangming Xiao:** Methodology, Conceptualization, Supervision, Writing – review & editing.

## Declaration of Competing Interest

The authors declare the following financial interests/personal relationships which may be considered as potential competing interests: Jie Wang reports financial support was provided by National Natural Science Foundation of China. Jie Wang reports financial support was provided by Key Research and Development Projects of Ningxia Province.

## Data availability

Data will be made available on request.

## Acknowledgments

This study is funded by the National Natural Science Foundation of China (42101355), the Key Research and Development Projects of Ningxia Province, China (2022BEG03050), and the Chinese Universities Scientific Fund (15053346, 10092004, 31051203).

## Appendix A. Supplementary data

Supplementary data to this article can be found online at <https://doi.org/10.1016/j.ecolind.2023.110737>.

## References

- Abatzoglou, J.T., Dobrowski, S.Z., Parks, S.A., Hegewisch, K.C., 2018. TerraClimate, a high-resolution global dataset of monthly climate and climatic water balance from 1958–2015. *Sci. Data* 5, 170191.
- Ahlström, A., Raupach, M.R., Schurgers, G., Smith, B., Arneeth, A., Jung, M., Reichstein, M., Canadell, J.G., Friedlingstein, P., Jain, A.K., Kato, E., Poulter, B., Sitch, S., Stocker, B.D., Viovy, N., Wang, Y.P., Wiltshire, A., Zaehe, S., Zeng, N., 2015. The dominant role of semi-arid ecosystems in the trend and variability of the land CO<sub>2</sub> sink. *Science* 348 (6237), 895–899.
- Andela, N., Liu, Y.Y., Van Dijk, A., De Jeu, R.A.M., McVicar, T.R., 2013. Global changes in dryland vegetation dynamics (1988–2008) assessed by satellite remote sensing: comparing a new passive microwave vegetation density record with reflective greenness data. *Biogeosciences* 10, 6657–6676.
- Andrade, B.O., Koch, C., Boldrini, I.L., Vélez-Martín, E., Hasenack, H., Hermann, J.-M., Kollmann, J., Pillar, V.D., Overbeck, G.E., 2015. Grassland degradation and restoration: a conceptual framework of stages and thresholds illustrated by southern Brazilian grasslands. *Natureza & Conservação* 13 (2), 95–104.
- Bai, J., Shi, H., Yu, Q., Xie, Z., Li, L., Luo, G., Jin, N., Li, J., 2019. Satellite-observed vegetation stability in response to changes in climate and total water storage in Central Asia. *Sci. Total Environ.* 659, 862–871.
- Bardgett, R.D., Bullock, J.M., Lavorel, S., Manning, P., Schaffner, U., Ostle, N., Chomel, M., Durigan, G., Fry, E.L., Johnson, D., Lavalée, J.M., Le Provost, G., Luo, S., Png, K., Sankaran, M., Hou, X., Zhou, H., Ma, L., Ren, W., Li, X., Ding, Y., Li, Y., Shi, H., 2021. Combatting global grassland degradation. *Nat. Rev. Earth Environ.* 2 (10), 720–735.
- Berdugo, M., Kéfi, S., Soliveres, S., Maestre, F.T., 2017. Plant spatial patterns identify alternative ecosystem multifunctionality states in global drylands. *Nat. Ecol. Evol. Develop.* 1, 1–10.
- Burrell, A.L., Evans, J.P., Liu, Y., 2017. Detecting dryland degradation using time series segmentation and residual trend analysis (TSS-RESTREND). *Remote Sens. Environ.* 197, 43–57.
- Burrell, A.L., Evans, J.P., Liu, Y., 2018. The impact of dataset selection on land degradation assessment. *Isprs J. Photogramm.* 146, 22–37.
- Burrell, A.L., Evans, J.P., De Kauwe, M.G., 2020. Anthropogenic climate change has driven over 5 million km<sup>2</sup> of drylands towards desertification. *Nat. Commun.* 11, 3853.
- Cetin, M., 2019. The effect of urban planning on urban formations determining bioclimatic comfort area's effect using satellitia imagines on air quality: a case study of Bursa city. *Air Quality Atmos. Health* 12 (10), 1237–1249.
- Cetin, M., Aksoy, T., Cabuk, S.N., Senyel Kurkcuoglu, M.A., Cabuk, A., 2021. Employing remote sensing technique to monitor the influence of newly established universities in creating an urban development process on the respective cities. *Land Use Policy* 109, 105705.
- Cetin, M., Adiguzel, F., Cetin, Z., 2022. Determination of the effect of urban forests and other green areas on surface temperature in Antalya. In: Suratman, M.N. (Ed.), *Concepts and Applications of Remote Sensing in Forestry*. Springer Nature Singapore, Singapore, pp. 319–336.
- Cetin, M., Sevik, H., 2016. Evaluating the recreation potential of Ilgaz Mountain National Park in Turkey. *Environ. Monit. Assess.* 188 (1).
- Chen, T., Bao, A., Jiapaer, G., Guo, H., Zheng, G., Jiang, L., Chang, C., Tuerhanjiang, L., 2019. Disentangling the relative impacts of climate change and human activities on arid and semiarid grasslands in Central Asia during 1982–2015. *Sci. Total Environ.* 653, 1311–1325.
- Chen, T., Tang, G., Yuan, Y., Guo, H., Xu, Z., Jiang, G., Chen, X., 2020. Unraveling the relative impacts of climate change and human activities on grassland productivity in Central Asia over last three decades. *Sci. Total Environ.* 743, 140649.
- D'Odorico, P., Bhattachan, A., Davis, K.F., Ravi, S., Runyan, C.W., 2013. Global desertification: drivers and feedbacks. *Adv. Water Resour.* 51, 326–344.
- de Beurs, K.M., Henebry, G.M., Owsley, B.C., Sokolik, I., 2015. Using multiple remote sensing perspectives to identify and attribute land surface dynamics in Central Asia 2001–2013. *Remote Sens. Environ.* 170, 48–61.
- Degerli, B., Cetin, M., 2022. Evaluation from rural to urban scale for the effect of NDVI-NDBI indices on land surface temperature, in Samsun, Turkey. *Turkish J. Agric. – Food Sci. Technol.* 10, 2446–2452.
- Duan, W., Zou, S., Chen, Y., Nover, D., Fang, G., Wang, Y.i., 2020. Sustainable water management for cross-border resources: the Balkhash Lake Basin of Central Asia, 1931–2015. *J. Clean. Prod.* 263, 121614.
- Evans, J., Geerken, R., 2004. Discrimination between climate and human-induced dryland degradation. *J. Arid Environ.* 57 (4), 535–554.
- Fensholt, R., Langanke, T., Rasmussen, K., Reenberg, A., Prince, S.D., Tucker, C., Scholes, R.J., Le, Q.B., Bondeau, A., Eastman, R., Epstein, H., Gaughan, A.E., Hellden, U., Mbwo, C., Olsson, L., Paruelo, J., Schweitzer, C., Seauquist, J., Wessels, K., 2012. Greenness in semi-arid areas across the globe 1981–2007—an Earth Observing Satellite based analysis of trends and drivers. *Remote Sens. Environ.* 121, 144–158.
- Gorelick, N., Hancher, M., Dixon, M., Ilyushchenko, S., Thau, D., Moore, R., 2017. Google Earth Engine: planetary-scale geospatial analysis for everyone. *Remote Sens. Environ.* 202, 18–27.

- Hall, D.K., Riggs, G.A., Salomonson, V.V., DiGirolamo, N.E., Bayr, K.J., 2002. MODIS snow-cover products. *Remote Sens. Environ.* 83 (1-2), 181–194.
- He, B., Wang, S., Guo, L., Wu, X., 2019. Aridity change and its correlation with greening over drylands. *Agric. For. Meteorol.* 278, 107663.
- Higginbottom, T.P., Symeonakis, E., 2014. Assessing land degradation and desertification using vegetation index data: current frameworks and future directions. *Remote Sens.-Basel* 6, 9552–9575.
- Hu, Z., Zhang, C., Hu, Q., Tian, H., 2014. Temperature changes in central Asia from 1979 to 2011 based on multiple datasets. *J. Clim.* 27, 1143–1167.
- Huete, A., Didan, K., Miura, T., Rodriguez, E.P., Gao, X., Ferreira, L.G., 2002. Overview of the radiometric and biophysical performance of the MODIS vegetation indices. *Remote Sens. Environ.* 83 (1-2), 195–213.
- Jabal, Z.K., Khayyun, T.S., Alwan, I.A., 2022. Impact of climate change on crops productivity using MODIS-NDVI time series. *Civil Eng. J.* 8, 1136–1156.
- Jiang, L., Jiapaer, G., Bao, A., Kurban, A., Guo, H., Zheng, G., De Maeyer, P., 2019. Monitoring the long-term desertification process and assessing the relative roles of its drivers in Central Asia. *Ecol. Ind.* 104, 195–208.
- Jiang, L., Bao, A., Jiapaer, G., Liu, R., Yuan, Y., Yu, T., 2022. Monitoring land degradation and assessing its drivers to support sustainable development goal 15.3 in Central Asia. *Sci. Total Environ.* 807, 150868.
- Jiang, L., Guli-Jiapaer, Bao, A., Guo, H., Ndayisaba, F., 2017. Vegetation dynamics and responses to climate change and human activities in Central Asia. *Sci. Total Environ.* 599–600, 967–980.
- Karnieli, A., Gilad, U., Ponzet, M., Svoray, T., Mirzadinov, R., Fedorina, O., 2008. Assessing land-cover change and degradation in the Central Asian deserts using satellite image processing and geostatistical methods. *J. Arid Environ.* 72 (11), 2093–2105.
- Koutroulis, A.G., 2019. Dryland changes under different levels of global warming. *Sci. Total Environ.* 655, 482–511.
- Kumar, D., Soni, A., Kumar, M., 2022. Retrieval of land surface temperature from landsat-8 thermal infrared sensor data. *J. Human, Earth, and Future* 3, 159–168.
- Li, Z., Chen, Y., Li, W., Deng, H., Fang, G., 2015. Potential impacts of climate change on vegetation dynamics in Central Asia. *J. Geophys. Res. Atmos.* 120 (24), 12345–12356.
- Li, C., Fu, B., Wang, S., Stringer, L.C., Wang, Y., Li, Z., Liu, Y., Zhou, W., 2021. Drivers and impacts of changes in China's drylands. *Nat. Rev. Earth Environ.* 2 (12), 858–873.
- Lian, X., Piao, S., Chen, A., Huntingford, C., Fu, B., Li, L.Z.X., Huang, J., Sheffield, J., Berg, A.M., Keenan, T.F., McVicar, T.R., Wada, Y., Wang, X., Wang, T., Yang, Y., Roderick, M.L., 2021. Multifaceted characteristics of dryland aridity changes in a warming world. *Nat. Rev. Earth Environ.* 2, 232–250.
- Lu, X., Wang, L., McCabe, M.F., 2016. Elevated CO<sub>2</sub> as a driver of global dryland greening. *Sci. Rep.-Uk* 6, 20716.
- Ma, X., Zhu, J., Yan, W., Zhao, C., 2021. Projections of desertification trends in Central Asia under global warming scenarios. *Sci. Total Environ.* 781, 146777.
- Mariano, D.A., Santos, C.A.C.D., Wardlow, B.D., Anderson, M.C., Schiltmeyer, A.V., Tadesse, T., Svoboda, M.D., 2018. Use of remote sensing indicators to assess effects of drought and human-induced land degradation on ecosystem health in Northeastern Brazil. *Remote Sens. Environ.* 213, 129–143.
- McLeod, A.L., 2005. Kendall rank correlation and Mann-Kendall trend test. *R Package Kendall* 602, 1–10.
- Meinshausen, M., Smith, S.J., Calvin, K., Daniel, J.S., Kainuma, M.L.T., Lamarque, J.-F., Matsumoto, K., Montzka, S.A., Raper, S.C.B., Riahi, K., Thomson, A., Velders, G.J.M., van Vuuren, D.P.P., 2011. The RCP greenhouse gas concentrations and their extensions from 1765 to 2300. *Clim. Change* 109 (1-2), 213–241.
- Mohammad, A., Wang, X., Xu, X., Peng, L., Yang, Y., Zhang, X., Myneni, R.B., Piao, S., 2013. Drought and spring cooling induced recent decrease in vegetation growth in Inner Asia. *Agric. For. Meteorol.* 178–179, 21–30.
- Nama, A.H., Abbas, A.S., Maatooq, J.S., 2022. Field and satellite images-based investigation of rivers morphological aspects. *Civil Eng. J.* 8, 1339–1357.
- Pace, G., Gutiérrez-Cánovas, C., Henriques, R., Boeing, F., Cássio, F., Pascoal, C., 2021. Remote sensing depicts riparian vegetation responses to water stress in a humid Atlantic region. *Sci. Total Environ.* 772, 145526.
- Petrie, M.D., Collins, S.L., Swann, A.M., Ford, P.L., Litvak, M.E., 2015. Grassland to shrubland state transitions enhance carbon sequestration in the northern Chihuahuan Desert. *Glob. Chang. Biol.* 21 (3), 1226–1235.
- Piao, S., Wang, X., Park, T., Chen, C., Lian, X.u., He, Y., Bjerke, J.W., Chen, A., Ciais, P., Tømmervik, H., Nemani, R.R., Myneni, R.B., 2020. Characteristics, drivers and feedbacks of global greening. *Nat. Rev. Earth Environ.* 1 (1), 14–27.
- Poulter, B., Frank, D., Ciais, P., Myneni, R.B., Andela, N., Bi, J., Broquet, G., Canadell, J. G., Chevallier, F., Liu, Y.Y., Running, S.W., Sitch, S., van der Werf, G.R., 2014. Contribution of semi-arid ecosystems to interannual variability of the global carbon cycle. *Nature* 509 (7502), 600–603.
- Ren, Q., He, C., Huang, Q., Shi, P., Zhang, D., Güneralp, B., 2022. Impacts of urban expansion on natural habitats in global drylands. *Nat. Sustainability* 5, 869–878.
- Reynolds, J.F., Smith, D.M.S., Lambin, E.F., Turner, B.L., Mortimore, M., Batterbury, S.P. J., Downing, T.E., Dowlatabadi, H., Fernández, R.J., Herrick, J.E., Huber-Sannwald, E., Jiang, H., Leemans, R., Lynam, T., Maestre, F.T., Ayarza, M., Walker, B., 2007. Global desertification: building a science for dryland development. *Science* 316 (5826), 847–851.
- Sahin, G., Cabuk, S.N., Cetin, M., 2022. The change detection in coastal settlements using image processing techniques: a case study of Korfez. *Environ. Sci. Pollut. Res.* 29 (10), 15172–15187.
- Schiemann, R., Lüthi, D., Vidale, P.L., Schär, C., 2008. The precipitation climate of Central Asia—intercomparison of observational and numerical data sources in a remote semiarid region. *Int. J. Climatol.* 28 (3), 295–314.
- Stevens, N., Lehmann, C.E.R., Murphy, B.P., Durigan, G., 2017. Savanna woody encroachment is widespread across three continents. *Glob. Chang. Biol.* 23 (1), 235–244.
- Sulla-Menashe, D., Gray, J.M., Abercrombie, S.P., Friedl, M.A., 2019. Hierarchical mapping of annual global land cover 2001 to present: The MODIS Collection 6 Land Cover product. *Remote Sens. Environ.* 222, 183–194.
- Varol, T., Atesoglu, A., Ozel, H.B., Cetin, M., 2023. Copula-based multivariate standardized drought index (MSDI) and length, severity, and frequency of hydrological drought in the Upper Sakarya Basin. *Nat. Hazards* 116 (3), 3669–3683.
- Venter, Z.S., Cramer, M.D., Hawkins, H.J., 2018. Drivers of woody plant encroachment over Africa. *Nat. Commun.* 9.
- Wan, Z.M., 2014. New refinements and validation of the collection-6 MODIS land-surface temperature/emissivity product. *Remote Sens. Environ.* 140, 36–45.
- Wang, L., Tian, F., Wang, Y., Wu, Z., Schurgers, G., Fensholt, R., 2018c. Acceleration of global vegetation greening from combined effects of climate change and human land management. *Glob. Chang. Biol.* 24 (11), 5484–5499.
- Wang, L., Jiao, W., MacBean, N., Rulli, M.C., Manzoni, S., Vico, G., D'Odorico, P., 2022. Dryland productivity under a changing climate. *Nat. Clim. Chang.* 12 (11), 981–994.
- Wang, J., Xiao, X., Qin, Y., Dong, J., Geissler, G., Zhang, G., Cejda, N., Alikhani, B., Doughty, R.B., 2017. Mapping the dynamics of eastern redcedar encroachment into grasslands during 1984–2010 through PALSAR and time series Landsat images. *Remote Sens. Environ.* 190, 233–246.
- Wang, J., Xiao, X., Qin, Y., Doughty, R.B., Dong, J., Zou, Z., 2018a. Characterizing the encroachment of juniper forests into sub-humid and semi-arid prairies from 1984 to 2010 using PALSAR and Landsat data. *Remote Sens. Environ.* 205, 166–179.
- Wang, J., Xiao, X., Zhang, Y., Qin, Y., Doughty, R.B., Wu, X., Bajgain, R., Du, L., 2018b. Enhanced gross primary production and evapotranspiration in juniper-encroached grasslands. *Glob. Chang. Biol.* 24 (12), 5655–5667.
- Wright, C.K., de Beurs, K.M., Henebry, G.M., 2012. Combined analysis of land cover change and NDVI trends in the Northern Eurasian grain belt. *Front. Earth Sci.* 6 (2), 177–187.
- Xiao, X., Boles, S., Liu, J., Zhuang, D., Frolking, S., Li, C., Salas, W., Moore, B., 2005. Mapping paddy rice agriculture in southern China using multi-temporal MODIS images. *Remote Sens. Environ.* 95 (4), 480–492.
- Xiao, X., Hagen, S., Zhang, Q., Keller, M., Moore, B., 2006. Detecting leaf phenology of seasonally moist tropical forests in South America with multi-temporal MODIS images. *Remote Sens. Environ.* 103 (4), 465–473.
- Xu, H.-J., Wang, X.-P., Zhang, X.-X., 2016. Decreased vegetation growth in response to summer drought in Central Asia from 2000 to 2012. *Int. J. Appl. Earth Obs.* 52, 390–402.
- Yao, J., Liu, H., Huang, J., Gao, Z., Wang, G., Li, D., Yu, H., Chen, X., 2020. Accelerated dryland expansion regulates future variability in dryland gross primary production. *Nat. Commun.* 11, 1–10.
- Yuan, Y.e., Bao, A., Liu, T., Zheng, G., Jiang, L., Guo, H., Jiang, P., Yu, T., De Maeyer, P., 2021. Assessing vegetation stability to climate variability in Central Asia. *J. Environ. Manag.* 298, 113330.
- Yucedag, C., Kaya, L.G., Cetin, M., 2018. Identifying and assessing environmental awareness of hotel and restaurant employees' attitudes in the Amasra District of Bartin. *Environ. Monit. Assess.* 190 (2).
- Zhang, G., Biradar, C.M., Xiao, X., Dong, J., Zhou, Y., Qin, Y., Zhang, Y., Liu, F., Ding, M., Thomas, R.J., 2018. Exacerbated grassland degradation and desertification in Central Asia during 2000–2014. *Ecol. Appl.* 28 (2), 442–456.
- Zhou, Y., Zhang, L., Fensholt, R., Wang, K., Vitkovskaya, I., Tian, F., 2015. Climate contributions to vegetation variations in central asian drylands: pre- and post-USSR collapse. *Remote Sens.-Basel* 7.
- Zhou, Y., Zhang, L., Xiao, J., Williams, C.A., Vitkovskaya, I., Bao, A., 2019. Spatiotemporal transition of institutional and socioeconomic impacts on vegetation productivity in Central Asia over last three decades. *Sci. Total Environ.* 658, 922–935.
- Zhu, S., Li, C., Shao, H., Ju, W., Lv, N., 2019. The response of carbon stocks of drylands in Central Asia to changes of CO<sub>2</sub> and climate during past 35 years. *Sci. Total Environ.* 687, 330–340.